UNIVERSIDAD DE GRANADA

Faculty of Science

BACHELOR´S DEGREE IN BIOTECHNOLOGY

BACHELOR´S DEGREE FINAL PROJECT

OPTIMIZATION OF A POSITIVE VALIDATION ASSAY BASED ON CHEMICAL DENATURATION EXPERIMENTS

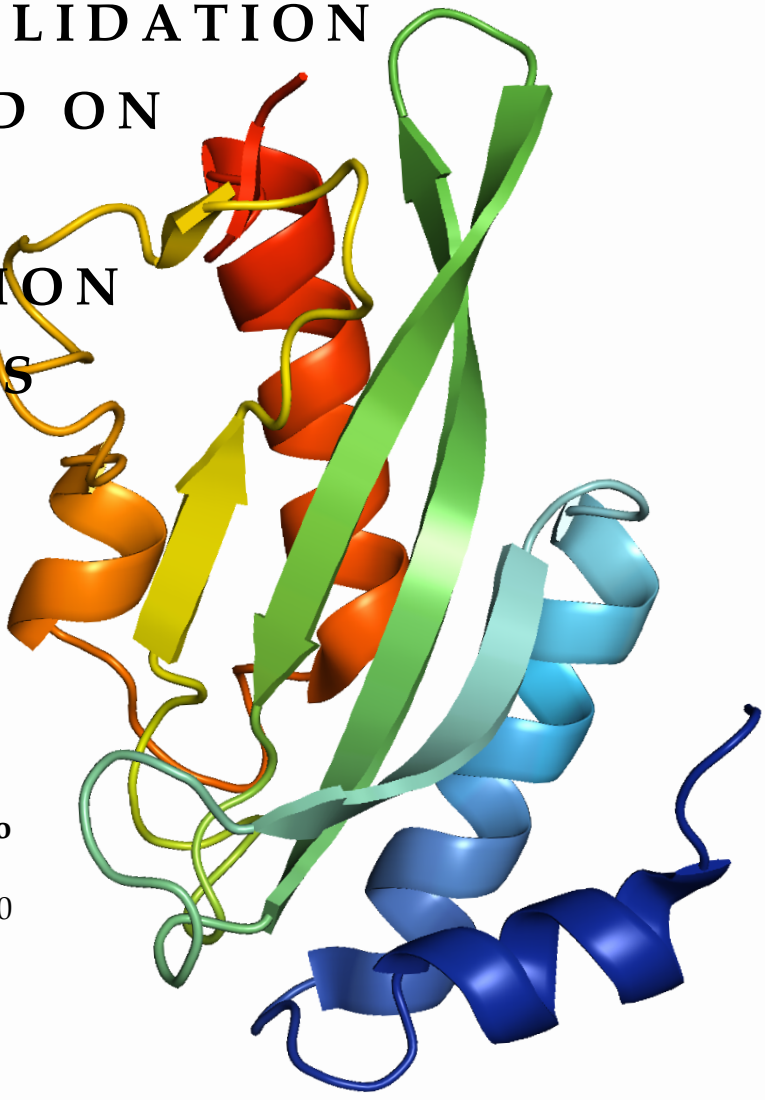

Presented by:
Mr. Raúl Carrillo Casado

Academic year 2019/2020

TABLE OF CONTENTS

ABSTRACT

Viral infectious diseases have been considered as extremely potential risks throughout human history. Vaccination or viral-directed antivirals have been proved ineffective as long-term treatments against highly mutable pathogens like RNA virus, including VIH, Marburg or Ebola. In the last decade, several studies have laid on the table the feasible targeting of human machinery recruited during viral infection as a way of disrupting viral cycle. The aim of this work was to validate the binding to the human ESCRT domain Tsg101-UEV of a non-peptidic ligand identified by in vitro massive campaigns, NIH-11. The binding was validated measuring the degree of stabilization of Tsg101-UEV in a chemical denaturation assay followed with intrinsic fluorescence measurements. The results showed a clear, but weak binding to Tsg101-UEV with a K_d on the micromolar range. The binding constant estimated here constitutes a starting point in the further thermodynamic explanation of this interaction, which will lead to an affinity optimization to turn the candidate into an effective broad-spectrum antiviral.

Key words: host-directed antivirals; virus budding; Tsg101-UEV domain; ligand binding affinity; chemical denaturation assay.

INTRODUCTION

1. Viral budding as a target in the development of broad-spectrum antivirals

Infectious diseases are among the top ten causes of death worldwide according to the World Health Organization (https://www.who.int/news-room/fact-sheets/detail/the-top-10-causes-of-death). Considering all their possible causes, viral infectious diseases represent, with two thirds of the current total infectious risks, the biggest impact on global health, being characterised by a high tendency to produce severe epidemics (Dye, 2014; Nii-Trebi, 2017).

It is at the beginning of a new decade, where we are, unfortunately, experimenting how the complex combination of both human and environmental factors can substantially aggravate the propagation of infectious diseases (Lederberg et al., 1992; Pavia, 2007). In fact, at this point of the pandemic, few individuals could deny the strength of the "enemy´s troops", even if we are talking about a "nanometric opponent ".

As strange as it sounds, this situation is only a shadow of a much bigger issue, which has walked with us throughout human history (Anthony S. Fauci, M.D., and David M. Morens & A, 2012; Morens et al., 2008). Centuries ago, we already had to face several infectious risks like Black Death , Smallpox and Measles (Nii-Trebi, 2017). For several decades, authors have been using the term "emerging or re-emerging diseases" (Lederberg et al., 1992), being a clear example the irruption of the virus SARS-CoV-2 (*Coronaviridae*) (Reina, 2020). Once a pathogen gets to infect a human organism, if we are not able to control it, it could become endemic or guarantee its continuity in global population, like Ebola virus (*Filoviridae*), Lassa fever virus (*Arenaviridae*) and HIV (*Retroviridae-Lentivirus*) (Bagcchi, 2020; Eisinger & Fauci, 2018; Ilunga Kalenga et al., 2019).

There is a special concern about enveloped retrovirus and RNA virus, specially *filovirus* and *arenovirus* families (Basler, 2017), as they are characterized for producing severe diseases that have led them to occupy the maximum health risk category according to the National Institute of Allergy and Infectious Diseases (NIAID) ranking. Nevertheless, due to the complexity of its impact, few of these biohazards can be immediately prevented by vaccine development (Drury et al., 2019; Oyston & Robinson, 2012). This fact has highlighted the urgent need to develop broad-spectrum antivirals, which are able to block viral cycle in any of its stages, and, as a result, control and even cure the infection once it is contracted.

This work is specifically focused in the viral budding step. This stage depends on the human ESCRT machinery, which is naturally presented in the host cell (Schmidt & Teis, 2012) and usually involved in multivesicular bodies (MVBs) formation. In their adaptation to the host, virus have achieved to recruit the ESCRT machinery through interactions between ESCRT proteins and short viral peptides called L-domains, which are highly conserved and shared by several virus (Martin-Serrano & Neil, 2011; Pornillos et al., 2002).

Currently, the L-domains whose interactions are better known are three (Martin-Serrano & Neil, 2011): P(T/S)AP L-domains recruit ESCRT-I complex through the interaction with the UEV domain of Tsg101; LYP$(x)_n$L L-domains bind to the V domain of the adaptor protein Alix, allowing the subsequent recruitment of the ESCRT-III complex through its protein CHMP4; PPxY L-domains bind the WW domains of Nedd4-like HECT ubiquitin ligase, which triggers the interaction with the other components of the ESCRT machinery.

The study of these mechanisms has brought to light the possibility of using the ESCRT machinery as an alternative target to block the virus proliferation, meaning a way of stopping the infection. For this reason, these interactions have been proposed as clear targets in the development of broad-spectrum antivirals, effective against different virus and, by being targeted against cellular proteins, they are less likely to develop resistance (Martinez et al., 2015). In the last years, several studies have proven this approach in the treatment of some infectious diseases like AIDS, Ebola or Marburg (Han et al., 2014; Tavassoli et al., 2008).

This Bachelor´s Degree Final Project belongs to a research line in development by FQM171 Group in the Physical-Chemistry Department of the University of Granada, currently funded by the State Plan BIO2016-78746 project. This project, in collaboration with MEDINA Foundation, is aimed at identifying non-peptidic inhibitors of viral budding by in vitro, in vivo and in silico screening of massive compounds and microbial extracts collections. In the context of this project, it has been possible to identify a set of molecules that block in vitro the interaction between Tsg101-UEV and L-domains type PTAP of Ebola and HIV-1. Furthermore, these compounds have shown inhibitory activity against viral budding in vivo, both in viral particles and full virus. A fundamental step in the characterisation of these compounds to prioritise those of bigger interest is to quantify their binding affinity and specificity. So far, because of the nature of these interactions, the measures performed by the research group with standard techniques (fluorescence titrations and differential scanning calorimetry) have not made possible the quantification of dissociation constants (or binding affinities).

The main goal of this project will be, therefore, to optimise an alternative method, based in the coupling of binding and denaturation equilibriums of Tsg101-UEV, to validate its binding to the ligands identified in previous in vitro massive campaigns, and to possibly estimate their dissociation constants (K_d).

2. Description of the human target evaluated: Tsg101-UEV domain

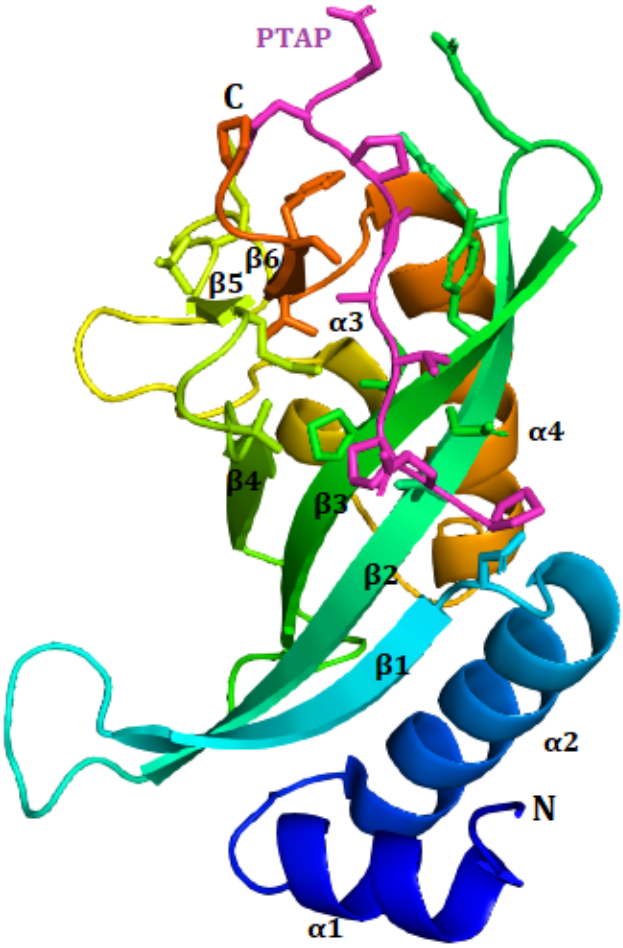

Figure 1. *Representation of Tsg101-UEV/PTAP interaction with the software Pymol*

Tsg101 (Tumor susceptibility gene 101) is a component of the ESCRT machinery, involved in the endosomal vesiculation/trafficking pathway (Yun et al., 2013). It is composed of several domains: an N-terminal UEV domain, a proline-rich region (PRR), a coiled coil (CC) region and a C-terminal α-helical/steadiness box (SB) domain.

The Tsg101-UEV domain folds into a typical (UBC)-like structure (SCOP classification), with four α-helices packed against one side of a four stranded anti-parallel β-sheet (**Figure 1**). As do the other UEV domains, Tsg101-UEV consists of a variant of ubiquitin E2 ligases, since it lacks both the cysteine catalytic residue and the two C-terminal α-helices (Palencia et al., 2006). It represents the binding site of the PTAP L-domain to the protein Tsg101 (Im et al., 2010) (**Figure 1**).

3. Main techniques applied in binding affinity studies of protein-ligand pairs

At present, there is an important number of well-stablished techniques used in binding affinity studies (Gao et al., 2020). The main techniques are summarized in **Table 1**.

Table 1. *Comparative of the most common techniques used in the determination of the binding affinities of protein-ligand, protein-protein pairs*

Technique	Basic principle	Advantages	Disadvantages	References
Isothermal Titration Calorimetry (ITC)	The amount of heat required to maintain the sample temperature varies with the binding to a ligand. Main technique.	- Complete and direct thermodynamic characterization of the system (ΔH, ΔS, Ka, ΔC_p, stoichiometry) - Minimum impact on the sample - High accuracy and reproducibility	- It requires too much high-purity sample. Low throughput. - It requires considerable preparation and time - Limited sensitivity	(Bouchemal, 2008; Du et al., 2016; Gao et al., 2020; Vuignier et al., 2010)
Spectroscopic Titrations (UV/Vis, DC, Fluorescence, RMN)	Change in the magnitude of a spectroscopic observable associated to the ligand binding	- Relatively simple - Low sample requirement	- Incomplete thermodynamic characterization, only estimation	(Greenfield, 2004; Mocz & Ross, 2013; Williamson, 2013)
Differential Scanning Calorimetry (DSC)	The amount of heat required to increase the sample temperature varies with the ligand binding	- High sensitivity - Label-free - It allows the determination of high Ka, greater than 10^{15} M^{-1}	- Low throughput - Irreversibility problems - Previous knowledge of the binding (ITC)	(Bruylants et al., 2005; Gao et al., 2020; Vuignier et al., 2010)
ThermoFluor (DSF)	The thermal stability of the protein increases with the ligand binding	- High throughput - Low sample requirement and fast performance - Both materials and equipment are affordable and readily available	- Considerable number of false positives and negatives - Irreversibility problems - It normally requires a label	(Bai et al., 2019; Douse et al., 2015; Gao et al., 2020; Kranz & Schalk-Hihi, 2011)

Normally, Spectroscopic Titrations represent the first approach, since, even if they don´t allow a complete characterization, they can be used to estimate binding affinities. Unfortunately, in our case, it has not been possible to apply this approach to the ligands identified, due to the signal deficiency between the free and bound state and to the presence of interferences in the bound state signal. Furthermore, it has been impossible to use ITC due to the high dilution heats observed, whose origin is yet to be clarified by the research group.

In addition to these disadvantages, we have to consider that in DSC and ThermoFluor assays, the affinity values are obtained at protein denaturation temperatures (T_m) (Bai et al., 2019; Bruylants et al., 2005). These temperatures are usually around 60ºC, so the affinity values obtained could not agree with those at physiological temperature (around 37ºC) (Schön et al., 2013). We would have to recalculate the value of the constant at the correct temperature from the Van´t Hoff equation, which implies previous knowledge of the enthalpy and heat capacity of both denaturation and binding process (Brandts & Lin, 1990). These thermodynamic parameters are difficult to determine in the same denaturation experiment and the extrapolation has a significant error associated (Waldron & Murphy, 2003).

(Schön et al., 2013) propose a method that, like DSC and ThermoFluor techniques, search for assessing ligand affinity indirectly, based on the protein stabilization resulting from the binding. What sets this method apart is that the protein denaturation is the result of a denaturant (isothermal conditions) and, the observable which will allow us to follow the process is the intrinsic fluorescence intensity change (label-free).

In this way, to validate the binding of Tsg101-UEV domain to the non-peptidic ligand NIH-11 and estimate its affinity (K_d), we will resort to the assays of (Schön et al., 2013), where they assess the effect of the ligand binding on the domain stability in chemical denaturation experiments, followed through intrinsic fluorescence spectroscopy.

AIMS OF THE PROJECT

In the next lines, I enumerate all the aims that I have addressed in the course of this research.

Aim 1: To optimise the chemical denaturation experiments of Tsg101-UEV.

Aim 2: To obtain chemical denaturation curves in the presence of different concentrations of the selected antiviral candidate.

Aim 3: To thermodynamically analyse the experimental results and estimate the binding affinity value (K_d).

WORK PLAN

Once the objectives have been presented, we have to mention the main steps in their approach.

Aim 1: To optimise the chemical denaturation experiments of Tsg101-UEV.

- Expression and purification of Tsg101-UEV using nickel affinity chromatography.
- Initial spectroscopic analysis of Tsg101-UEV to identify the optimal technique and conditions to perform the chemical denaturation experiments.
- Obtaining Tsg101-UEV chemical denaturation curves in order to determine and improve the reproducibility of the method.

Aim 2: To obtain chemical denaturation curves in the presence of different concentrations of the selected antiviral candidate.

- Obtaining Tsg101-UEV chemical denaturation curves in the presence of NIH-11.

Aim 3: To thermodynamically analyse the experimental results and estimate the binding affinity value (K_d).

- Thermodynamic analysis of the experimental results and binding affinity estimation.

METHODOLOGY

- **<u>Aim 1</u>:** To optimise the chemical denaturation experiments of Tsg101-UEV.

1.1. Expression and purification of Tsg101-UEV using nickel affinity chromatography.

Both the expression and purification of Tsg101-UEV were previously done to my personal contribution. In the purification process, they used a nickel affinity chromatography, based in the interaction of the polyhistidine tail in the protein construction (highlighted in red) and the nickel groups in the column.

At the end of the process, the protein was obtained at a quantity (tens of mg) and purity (> 95%) high enough to perform the biophysical studies. The molecular weight of the protein construction was 17938.8 g/mol.

The final sequence obtained for Tsg101-UEV is the following:

MRGSHHHHHHGMASMAVSESQLKKMVSKYKYRDLTVRETVNVITLYKDLKPV
LDSYVFNDGSSRELMNLTGTIPVPYRGNTYNIPICLWLLDTYPYNPPICFVKPTSS
MTIKTGKHVDANGKIYLPYLHEWKHPQSDLLGLIQVMIVVFGDEPPVFSRP

This sequence made possible to obtained the molar extinction coefficient at 280 nm, which is 24410 $M^{-1} \cdot cm^{-1}$ (Pace et al., 1995).

1.2. Initial spectroscopic analysis of Tsg101-UEV to identify the optimal technique and conditions to perform the chemical denaturation experiments.

1.2.1. Choosing the best spectroscopic technique to follow the chemical denaturation of Tsg101-UEV

The experiments aimed at choosing the best technique to follow the denaturation process were also previously done to my personal contribution. In them, native and denatured states had to be registered and, the following aspects were analysed:

- The magnitude of the signals from native and denatured states
- The difference between the spectrums of both states
- The signal-to-noise ratio

It was possible to follow the denaturation process through the measurement of the intrinsic fluorescence from Trp 75 and 117 residues, with a constant concentration for Tsg101-UEV of 2.5 μM (**Figure 3**). It was agreed to register the complete fluorescence spectrum from

285 to 400 nm and, to take the ratio between the wavelengths of 320 and 360 nm (wavelengths of maximum intensity for the native and denatured states, respectively) as the fluorescence value, in order to correct any possible fluctuation in the protein concentration in each urea solution.

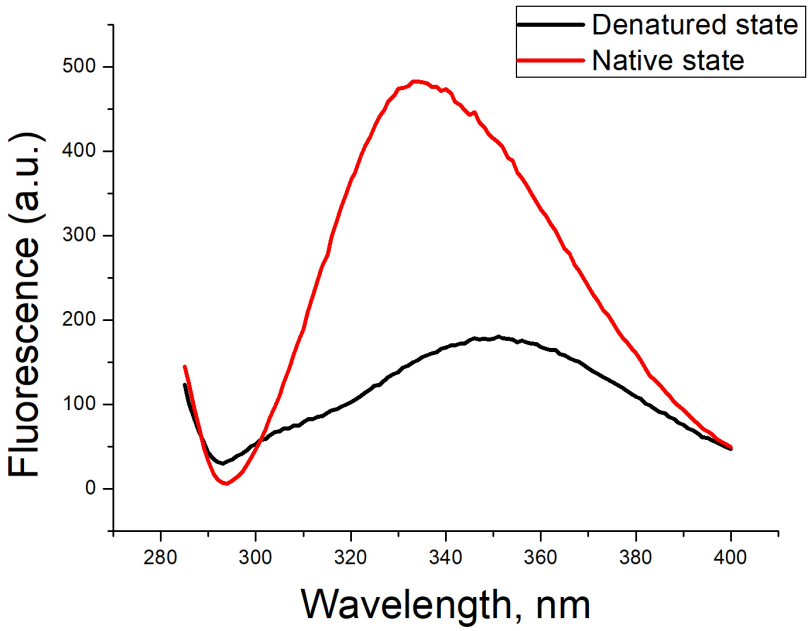

Figure 3. *Comparative of the differences between the spectrums of the native and denatured states*

1.2.2. Choosing the best experimental conditions and reagents for the selected technique

In the next paragraphs, I summarize the previous tests, performed before my personal contribution, in order to choose the best reagents and their proportion in each solution:

- DMSO (dimethyl sulfoxide) is an usual organic solvent in compound collections , since it allows the solubilization of a great variety of organic compounds (Balakin et al., 2004; Tjernberg et al., 2006). Previous studies indicated that the minimum percentage required to guarantee both the solubility of the compounds and the stability of the protein was an 8%.

- Earlier studies pointed out that the optimal pH value in order to guarantee Tsg101-UEV solubility was 3. Nevertheless, to be able to extrapolate the results to physiological conditions, it was necessary to maintain a pH of 7 during all the experiments. These pH conditions asked for a buffer based in Na_2HPO_4 and NaH_2PO_4 with a concentration of 50 mM.

- The denaturing agent selected was urea, since Tsg101-UEV can be completely denatured in its presence. Furthermore, being an uncharged molecule makes possible to work at higher concentrations without the risk of also increasing the ionic strength, and as a result the instability of the protein, which is not the case of guanidinium chloride (Monera et al., 1994).

1.3. Preparation of Tsg101-UEV solution

1.3.1. Tsg101-UEV dialysis

Owing to the requirement of a physiological pH (around 7), so that the stability of the protein is as close as possible to that in physiological conditions, the step before the concentration measurement was Tsg101-UEV dialysis. Tsg101-UEV construction was frozen at -80 ºC in glycine pH 3 buffer, so we had to change it to a Na-Pi 50mM pH 7 buffer.

a. Preparation of Na-Pi 50 mM pH 7 buffer

5.88 g of NaH_2PO_4 and 10.2 g of Na_2HPO_4 were weighed and added to a 2 L beaker. A volume of water close to 2 L was added and the solution was put into magnetic agitation. Once the salts were dissolved, the pH of the solution was measured and showed a value close to 7, so it did not require any adjustment. This volume was transferred to a volumetric flask, where the final volume was precisely completed to two litres.

The buffer was distributed in two beakers of 1L for each dialysis step and, also, one part of this volume (around 100 mL) was filtered with a filter of 0.45 µm of pore size, in order to be used later in all the following solutions.

b. Preparation of the dialysis sack

The experiments were performed using a frozen stock solution at a concentration of 280 µM, which first required a defrosting time in ice. The dialysis sack prepared had a length of 7 cm and a pore size of 6-8 KDa (significantly below the 18 KDa of the protein´s molecular weight, minimising the loss of protein), also, the sack was hydrated in mili-Rho water. Considering the dilution that usually occurs in dialysis, 714 µL of the solution at 280 µM were introduced in the sack, so that, when the total volume was completed to 1 mL, the final solution would be concentrated enough (200 µM approximately) to prepare the final solution at 150 µM.

The dialysis sack was put in the first dialysis litre into magnetic agitation for 5 h at 4ºC. After this time, the sack was changed to the second dialysis litre in the same agitation and temperature conditions for 10 h (overnight).

1.3.2. Determination and adjustment of Tsg101-UEV final concentration

For the measurement of protein concentration, the most common equipment used is an UV-Visible Absorbance Spectrophotometer. It is the presence of chromophores (like aromatic residues, prosthetic groups, etc) in a molecule, which allows its absorbance in this region of the electromagnetic spectrum (Schmid & Beer, 2001). In this case, the absorbance of the Tsg101-UEV domain in the UV-Visible range is mainly due to its Tyrosine residues (Im et al., 2010).

The first concentration measurement of Tsg101-UEV was done to the solution recovered from the dialysis sack. The absorbance value was measured at 280 nm (wavelength where the Tryptophan residues show their maximum absorbance). This wavelength is routinely used in the measurement of protein concentration, since proteins have their absorbance spectrum dominated by the Tryptophan residues. The measurement required a cuvette with an optic path of 0.1 cm and the molar extinction coefficient at 280 nm, which is 24410 $M^{-1} \cdot cm^{-1}$.

The measurement of the buffer absorbance is routinely previous to the measurement of the solution absorbance. This step is necessary to subtract the buffer spectrum from the solution spectrum, so that we can only obtain the protein contribution, making the interpolated protein concentration as real as possible (**Figure 4**).

Another fundamental aspect would be checking the absence of protein precipitate in the solution, especially considering that the pH is not optimal. This phenomenon is perceptible when there is an increase of absorbance at the final part of the spectrum, receiving the name of scattering (Mäntele & Deniz, 2017). Considering this risk, prior to the measurement, the sample was centrifugated for a short period, with the aim of removing any possible aggregation. The absence of scattering after the centrifugation step is shown in **Figure 4**.

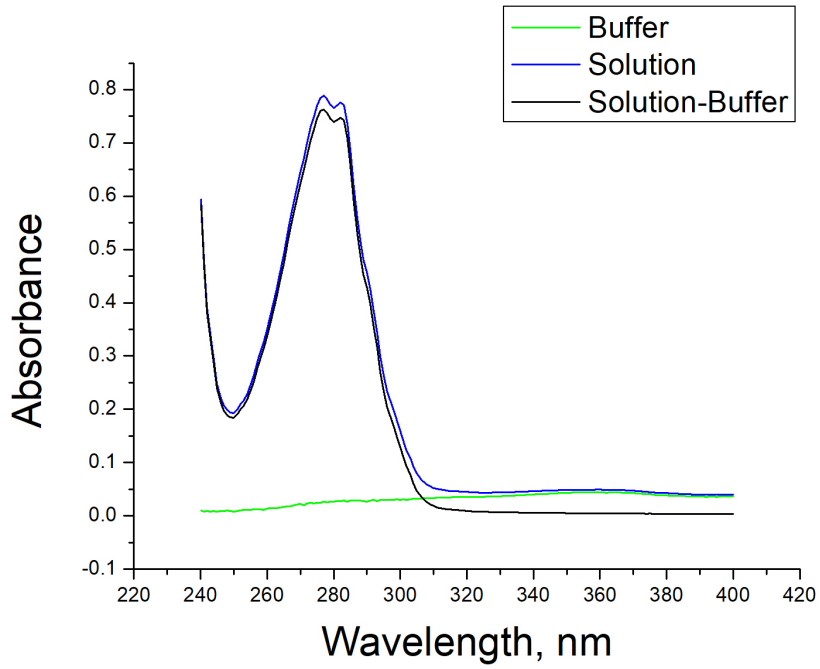

Figure 4. *Absorbance of the Tsg101-UEV solution at 150 µM*

Once we obtain the absorbance value, it is related to concentration through Lambert-Beer Law:

$$A_{280} = \varepsilon_{280} \cdot l \cdot c \; ; \; c = \frac{A_{280}}{\varepsilon_{280} \cdot l}$$

, being A_{280} the absorbance at 280 nm, l the optical path, ε_{280} the molar extinction coefficient at 280 nm and c the protein concentration.

With this first measurement of the protein concentration, the actual initial concentration was checked. Subsequently, the buffer volume required to dilute the sample to 150 µM was determined through a molar stoichiometry relation, considering that initial concentration.

After this last dilution, another measurement of the protein concentration was performed to verify that the final solution had a concentration of 150 µM. The only difference in this step was that we used a cuvette with an optical path of 0.2 cm, because the dilution of the sample minimised the risk of having an absorbance value out of the lineal range stablished for the Lambert-Beer Law (Mäntele & Deniz, 2017).

1.4. Preparation of urea stock solution

To obtain an urea solution at 10 M, 60 g of urea were weighed and dissolved in a volume of 100mL with miliQ water. The solution was put in a bain-marie and into magnetic agitation, to ease the dissolution of the salt in water.

During the dissolution process, 6 g of AG501-X8 resin were weighed and added to the solution once it reached room temperature again. This resin works removing from the solution any urea-derived reactive species.

One hour later, the mixture was put into a PD10 column, in order to remove through molecular exclusion any small impurities like salt residues, and the elutions, which contained the urea solution finally purified and separated from the resin, were collected.

The next step was preparing the Na-Pi 50 mM pH 7 buffer in two parts, which meant adding in one clean beaker 0.225 g of Na_2HPO_4 and in another 0.147 g of NaH_2PO_4. Then, a volume of 25 mL of the purified urea solution was added in both beakers. The mixture of both volumes was put into agitation and, when the salts were dissolved, the pH was measured and show a value of practically 7.

The final urea solution was filtered using a filter with a pore size of 0.45 µm, and then the total volume was divided in volumes of 5 mL, distributed in Falcons tubes of 15 mL.

The real urea concentration was determined with accuracy through the measurement of the refraction index (n) of the solution using a refractometer. For this purpose, a volume of 20 µL was taken using a Gilson pipette of 20 µL and put on the interior surface of the refractometer, previously cleaned and dried. To read the refraction index, you must place the light entry to a source of natural or artificial light. By doing this, we can see the level of refraction in the scale between the bright and dark zone. Then, we only have to adjust the clarity of the line, through the turn of a screw, to be able to see more clearly the exact value. After this procedure, we obtained a refraction index that, according to the equation proposed by (Warren & Gordon, 1966),

$$C_{urea} = 117.66 \cdot (\Delta n) + 29.753 \cdot (\Delta n)^2 + 185.56 \cdot (\Delta n)^3$$

represents an urea concentration of 9.57 M.

Finally, all the falcons were labelled and set at -20ºC for their later use in the denaturation experiments.

1.5. Obtaining Tsg101-UEV chemical denaturation curves

1.5.1. Preparation of the solutions at different urea concentrations

For the preparation of the experiments, a total number of 28 solutions were prepared at different increasing concentrations of urea (Schön et al., 2013).

The range of the twenty-eight solutions went from 0 to 8.5 M of urea. Except from 0 M to 3.5 M, where the difference between each point was of 0.5 M, between the rest of points the increase was of 0.25 M, with the aim of obtaining a better definition in the curve, especially in the transition zone.

In the **Table 2** the volumes of each component are shown for a total volume of 300 µL in each solution.

Table 2. *Volumes of all the components in each urea solution for the denaturation of Tsg101-UEV in the absence of NIH-11*

Point	[Urea]	µL TSG	µL UREA	µL Buffer	µL DMSO	Point	[Urea]	µL TSG	µL UREA	µL Buffer	µL DMSO
1	0	5	0	271	24	15	5.25	5	165	106	24
2	0.5	5	16	255	24	16	5.5	5	172	99	24
3	1	5	31	240	24	17	5.75	5	180	91	24
4	1.5	5	47	224	24	18	6	5	188	83	24
5	2	5	63	208	24	19	6.25	5	196	75	24
6	2.5	5	78	193	24	20	6.5	5	204	67	24
7	3	5	94	177	24	21	6.75	5	212	59	24
8	3.5	5	110	161	24	22	7	5	219	52	24
9	3.75	5	118	153	24	23	7.25	5	227	44	24
10	4	5	125	146	24	24	7.5	5	235	36	24
11	4.25	5	133	138	24	25	7.75	5	243	28	24
12	4.5	5	141	130	24	26	8	5	251	20	24
13	4.75	5	149	122	24	27	8.25	5	259	12	24
14	5	5	157	114	24	28	8.5	5	266	5	24

Once all the solutions at different urea concentrations were prepared, they were put into incubation at 25ºC for 24 h, looking for the system to reach the equilibrium. This incubation step is fundamental, since all the thermodynamic model that we will later apply in the data analysis is based on our system having reached the equilibrium between the native and denatured states (Schön et al., 2013).

1.5.2. Measurement of the fluorescence spectrums for each urea concentration

After the 24 h of incubation, when we estimate that our system has reached the equilibrium, the next step was to measure the fluorescence of each solution.

The measurement was made individually in ascending order of urea concentration. The three first concentrations (0, 0.5 and 1 M of urea) were previously centrifugated for 3 min at 14000 rpm to remove any precipitate produced by the smaller urea concentration. The solutions with a bigger urea concentration were homogenized with the pipette before taking the volume of measure, specifically 75 µL.

The measurement of the real urea concentration was performed simultaneously with the fluorescence scan, employing the same method described in the section 1.4.

- **Aim 2:** To obtain chemical denaturation curves in the presence of different concentrations of the selected antiviral candidate.

2.1. Preparation of NIH-11 solution

NIH-11 was supplied freeze-dried, so its preparation comprised, firstly, dissolving the compound in DMSO. The dissolution required weighing 2.19 g of the dried compound and adding a volume of 192 µL of DMSO to have a final concentration of 25 mM.

The expected effect because of the addition of the ligand is an increase in the urea concentration at the transition mid-point, due to the stabilization of the native state (Schön et al., 2013). This effect depends on the binding affinity (K_d) and the ligand concentration. For our system, the binding affinity was not expected to be very strong, therefore, based on the bibliography, we agreed to put an excess in the ligand concentration forty times bigger than the protein concentration, to make it possible to see a significant change.

In this way, the concentration of an intermediate solution from the stock solution of NIH-11 was calculated, so that adding 24 µL of the stock it was possible to obtain a final concentration of 100 µM in the 300 µL of each solution. This concentration is clearly forty times bigger than the Tsg101-UEV concentration of 2.5 µM, justified in the section 1.2.1.

2.2. Obtaining Tsg101-UEV chemical denaturation curves in the presence of NIH-11

To obtain the denaturation curves of Tsg101-UEV in the presence of NIH-11, we followed the same procedure described in the section 1.5 to prepare the solutions as well as to measure the fluorescence data and the urea real concentrations.

- **<u>Aim 3</u>:** To thermodynamically analyse the experimental results and estimate the binding affinity value (K_d).

3.1. Analysis of the chemical denaturation curves

Once the denaturation process of each solution has reached the equilibrium, we will find two majority populations defined through their equilibrium constant of unfolding, K_U (Privalov, 1979).

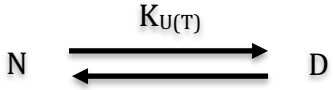

In this way, the final observable measured will be the average of both populations, which can be expressed in the following manner:

$$< Y >= P_N Y_N + P_U Y_U \quad \text{(Eq.1)}$$

, being P_N y P_U, the populations of the native and unfolded states and, Y_N and Y_U, the fluorescence signals of each state, respectively.

If we want to define the populations of each state, we can do it on the basis of their Gibbs Free Energy according to Statistical Thermodynamics.

$$P_N = \frac{1}{1 + e^{-\Delta G_U/RT}} \; ; \; P_U = \frac{e^{-\Delta G_U/RT}}{1 + e^{-\Delta G_U/RT}} \quad \text{(Eq.2)}$$

$$P_N + P_U = 1 \quad \text{(Eq.3)}$$

, being ΔG_U the protein stability (change in Gibbs Free Energy between the native and unfolded state), R the ideal gas constant (8.314 J/mol K) and T the operating temperature of the experiments (298.15 K).

Considering that the population fractions of each state are calculated as the ratio of each individual population to the total, if our system meets the approximation of a two states model and the principle of mass conservation, the addition of both fractions must be 1 (Eq.3)

Taking into account equations 2 and 3, equation 1 takes the following expression.

$$< Y >= \frac{Y_N + Y_U\, e^{-\Delta G_U / RT}}{1 + e^{-\Delta G_U / RT}} \qquad \text{(Eq.4)}$$

In general, based in experimental obervations, the stability of a protein can be related to the denaturant concentration through the next equation:

$$\Delta G_U = \Delta G_U{}^o - mC \qquad \text{(Eq.5)}$$

, being ΔG_U the protein stability, now, in the presence of the denaturing agent, $\Delta G_U{}^0$ the stability in the absence of the denaturant, m the dependence of the stability with the denturant concentration, that in turn depends on the protein surface exposed to the solvent (Myers et al., 1995), and C the denaturant concentration.

If we consider in Equation 4 that dependence of some parameters with the denaturant concentration, we obtain the next expression:

$$< Y >= \frac{(Y_N + a_N C) + (Y_U + a_U C)\, e^{-(\Delta G_U^0 - mC)/RT}}{1 + e^{-(\Delta G_U^0 - mC)/RT}} \qquad \text{(Eq.6)}$$

, being a_N and a_U the constants that relate the signal of the native and unfolded states with the denaturant concentration.

As stated above in the section 1.2.1., the data from the observable that will be really used in Equation 5 as $< Y >$ is the ratio between the fluorescence intensity at the wavelengths of 320 and 360 nm. This ratio will be used with the aim of correcting any possible fluctuation in the protein concentration in each replica, which will allow their later comparison. And, also, it will be fundamental that the urea concentration used is the real, which will be calculated according to (Warren & Gordon, 1966).

Finally, this model will be inserted in the software Origin, in order to obtain the fitting curve for our experimental data.

3.2. Thermodynamic model aimed at the determination of binding affinities from chemical denaturation curves data

Following the same premises that our system under study has two accesible states and, in addition, that the ligand binds preferentially to the native state, as it is our case. The binding to a protein can be expressed in terms of an equilibrium between two possible states:

$$N + L \underset{K_{d(T)}}{\rightleftharpoons} NL$$

This equilibrium is defined by the dissociation constant (K_d), which is inversely related to the association constant (K_a).

$$K_d = \frac{1}{K_a} \quad \text{(Eq.7)}$$

In the same way that we have defined the stability of a protein being influenced by a denaturant, the change in the stability of our system due to the binding of a ligand can be defined in this manner:

$$\Delta G_L^o = \Delta G_U^0 + RT \ln(1 + \frac{[L]}{K_d}) \quad \text{(Eq.8)}$$

, being ΔG_L^o the stability of the system in the presence of the ligand and ΔG_U^0 the stability in its absence, both in the absence of denaturant (^{0}), [L] the concentration of free ligand and K_d the dissociation constant.

Taking into consideration the presence of the ligand in the chemical denaturation experiments, we can rewrite the equation 5 in this manner:

$$\Delta G_L = \Delta G_L^o - m_L C \quad \text{(Eq.9)}$$

, being the subscript $_L$ a reference to the same parameters in equation 5, but in the presence of the ligand.

We can go further and integrate the equation 8 in equation 9 (Schön et al., 2013), obtaining the next expression:

$$\Delta G_L = \Delta G_U^0 + RTln(1 + \frac{[L]}{K_d}) - m_L C \quad \text{(Eq.10)}$$

By reordering equation 10, we can obtain the first equation for the K_d:

$$K_d = \frac{[L]}{e^{(\frac{\Delta\Delta G^o}{RT} - 1)}} \quad \text{(Eq.11)}$$

, being $\Delta\Delta G^o$ equal to $\Delta G_L^o - \Delta G_U^0$.

These expressions will allow us to determine the binding constant from the chemical denaturation experiments, which can be performed at different ligand concentrations. Nevertheless, we face the problem that the parameters which influence K_d are not easily calculable. For this reason, the authors propose two modifications of the equation, to express it on the basis of more accessible parameters through the fitting of the chemical denaturation curve.

In the first place, they express $\Delta\Delta G^o$ as $\Delta C_{1/2}$, the difference between $C_{1/2}$ in the presence and in the absence of the ligand. $C_{1/2}$ is the urea concentration at the inflection point of our denaturation curve, where the native and denatured states coincide, implying this that $\Delta G = 0$.
In the second place, they express the equation based on the total ligand and protein concentration (not free), parameters which are easier to determine.

Including all these changes, the final equation for K_d gets the following aspect:

$$K_d = \frac{[L_T](1+F) - F[P_T]}{F(1+F)} \quad \text{(Eq.12)}$$

, being $F = \exp\left(\frac{m_L \Delta C_{1/2}}{RT}\right) - 1$

The parameter m_L was directly obtained from the fitting of the denaturation curve of Tsg101-UEV in the presence of NIH-11, performed by Origin. However, the calculation of $\Delta C_{1/2}$ required an indirect analysis of the fitting parameters in the absence and in the presence of NIH-11. From these parameters it was possible to simulate in Origin the experimental curves with a total of 600 points in a range from 0 to 8.5 M of urea, in order to obtain a bigger accuracy. Then, the simulation curves were derived and the $C_{1/2}$ value agreed with the absolute minimum of the curve.

RESULTS AND DISCUSSION

- **Determination and evaluation of the inner reproducibility of the replicas**

The first set target was to assess the inner reproducibility of the experiments in the absence and in the presence of NIH-11. This step was fundamental to assess the accuracy of the fitting parameters for replicas of the same composition, but prepared both with different reagents and in independent days, with respect to the one theoretically due to the only presence of the ligand NIH-11.

- **Tsg101-UEV chemical denaturation curves in the absence of NIH-11**

A total number of four replicas were performed, the first of them was an initial test and the rest were a minimum of three replicas which allowed to obtain a statistically significant value of $C_{1/2}$ and m (**Figure 5**).

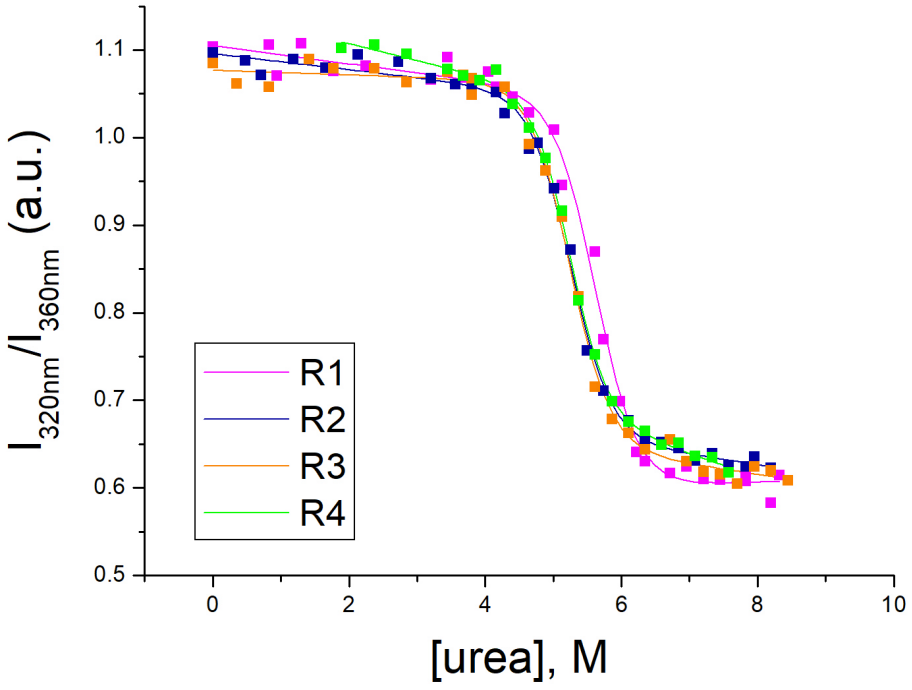

Figure 5. *Collection of the fitting curves in the absence of NIH-11*

The set of fitting parameters obtained after the analysis of the four replicas, together with the errors associated to their calculus, are summarised independently in **Table 3.**

Table 3. *Collection of the fitting parameters in the absence of NIH-11*

Replica	**1**	**2**	**3**	**4**
m, (J/mol)·M^{-1}	**-8000** ± 1000	**-8400** ± 800	**-8400** ± 800	**-9200** ± 800
a_n, M^{-1}	-0.010 ± 0.004	-0.009 ± 0.003	-0.003 ± 0.003	-0.019 ± 0.004
a_d, M^{-1}	0.00 ± 0.01	-0.01 ± 0.01	-0.01 ± 0.01	-0.03 ± 0.01
Y_n	1.10 ± 0.01	1.10 ± 0.01	1.08 ± 0.01	1.15 ± 0.01
Y_u	0.6 ± 0.1	0.7 ± 0.1	0.7 ± 0.1	0.8 ± 0.1
T, K	298	298	298	298
ΔG_U^0, J/mol	46000 ± 6000	44000 ± 4000	44000 ± 4000	48000 ± 4000

All the parameters collected in **Table 3** were directly obtained from the fitting of the denaturation curves in Origin, which also provides an estimation of their error.

In principle, all the fitting parameters obtained for each replica agree with those previously obtained for other small globular proteins, whose stability is usually marginal, specifically from 21 to 63 KJ/mol (Pace, 1990). Furthermore, the coherence of the results is also maintained in the replica 4, which had an experimental design slightly different to the rest of replicas due to the scarcity of reagents, which supports the robustness of the method.

Once the coherence of the fitting parameters for each replica was assessed, we studied the reproducibility of the method in the calculation of each individual $C_{1/2}$ and their mean value.

The calculation of $C_{1/2}$ was done as it was previously described in the section 3.2. of the methodology (**Figure 6**).

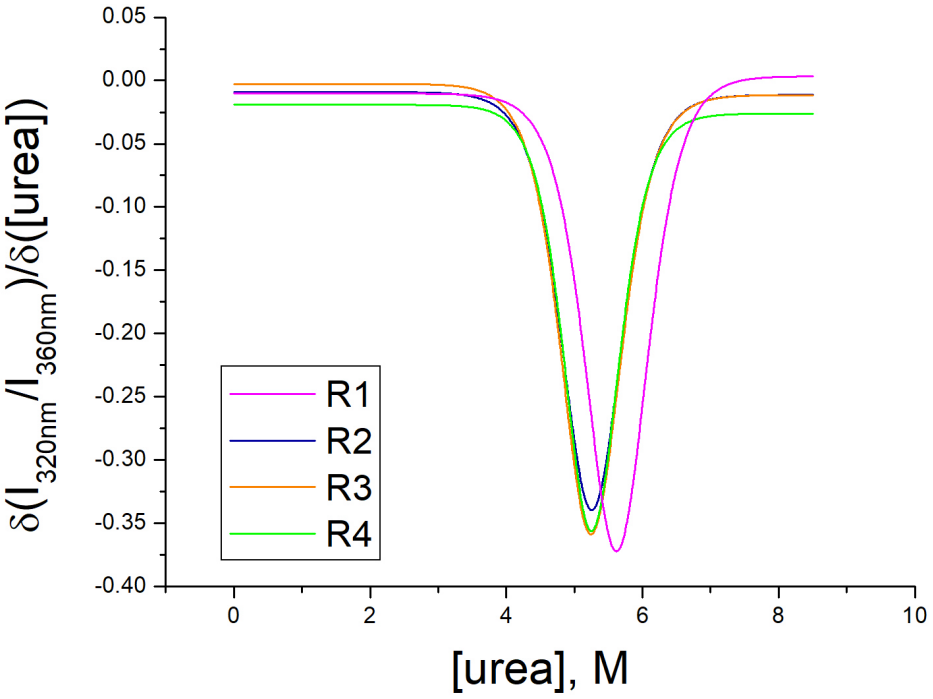

Figure 6. Derivatives of the simulation curves for each replica in the absence of NIH-11

The $C_{1/2}$ values obtained from the absolute minimums are summarised in **Table 4**.

Table 4. *$C_{1/2}$ values obtained for each replica in the absence of NIH-11*

Replica	**1**	**2**	**3**	**4**
$C_{1/2}$, M	**5.62**	**5.25**	**5.25**	**5.25**

In the replica 1, considered as a preliminary test, we obtained a significantly different value to the rest of replicas. Nevertheless, we saw that the later replicas, whose preparation was already optimised, presented a value of 5.25 ± 0 M, practically identical based on the accuracy of Origin.

- **Tsg101-UEV chemical denaturation curves in the presence of NIH-11**

Following the same analysis procedure that in the denaturation curves in the absence of NIH-11, we obtained the non-linear fitting of the four replicas (**Figure 7**). The first replica, as well as in the previous case, was performed as a preliminary test to optimise the preparation and the measurement of the solutions.

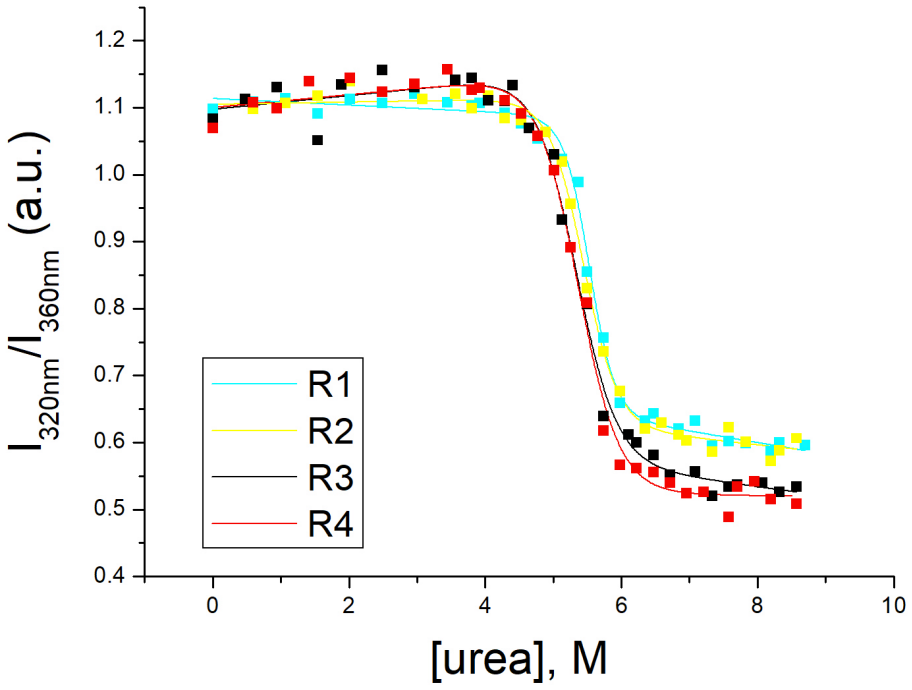

Figure 7. Collection of the fitting curves in the presence of NIH-11

All the fitting parameters obtained are summarised in **Table 5.**

Table 5. *Collection of the fitting parameters in the presence of NIH-11*

Replica	**1**	**2**	**3**	**4**
m_L, (J/mol)·M^{-1}	**-13000** ± 2000	**-9900** ± 900	**-8000** ± 1000	**-8000** ± 900
a_n, M^{-1}	-0.005 ± 0.003	0.002 ± 0.003	0.010 ± 0.005	0.010 ± 0.005
a_d, M^{-1}	-0.02 ± 0.01	-0.01 ± 0.01	-0.01 ± 0.01	-0.00 ± 0.01
Y_n	1.11 ± 0.01	1.10 ± 0.01	1.10 ± 0.01	1.10 ± 0.01
Y_u	0.7 ± 0.1	0.7 ± 0.1	0.6 ± 0.1	0.5 ± 0.1
T, K	298	298	298	298
ΔG_U^0, J/mol	73000 ± 9000	54000 ± 5000	45000 ± 6000	44000 ± 5000

The values obtained in the presence of NIH-11 were compared with those obtained in the absence. This comparative made us see that the dependence with the denaturant and the fluorescence signals stayed very similar in both conditions. It did not happen to be the same for the parameters m and ΔG_U^0, maybe due to the error in the preparation of the stock solution of NIH-11 from which we took the volume to prepare the replicas 3 and 4.

This error made that the two last replicas were at a concentration of 60 µM, lower than the concentration of 100 µM of the replicas 1 and 2. In this way, replicas 1 and 2 did fulfil the proportion of 40x with respect to Tsg101-UEV, while the other two replicas presented a lower proportion, specifically 24x.

To study the possible effect of this difference in ligand concentration in the final values for $C_{1/2}$, we determined these values for each replica following the procedure previously described for the replicas in the absence of NIH-11 (**Figure 8**).

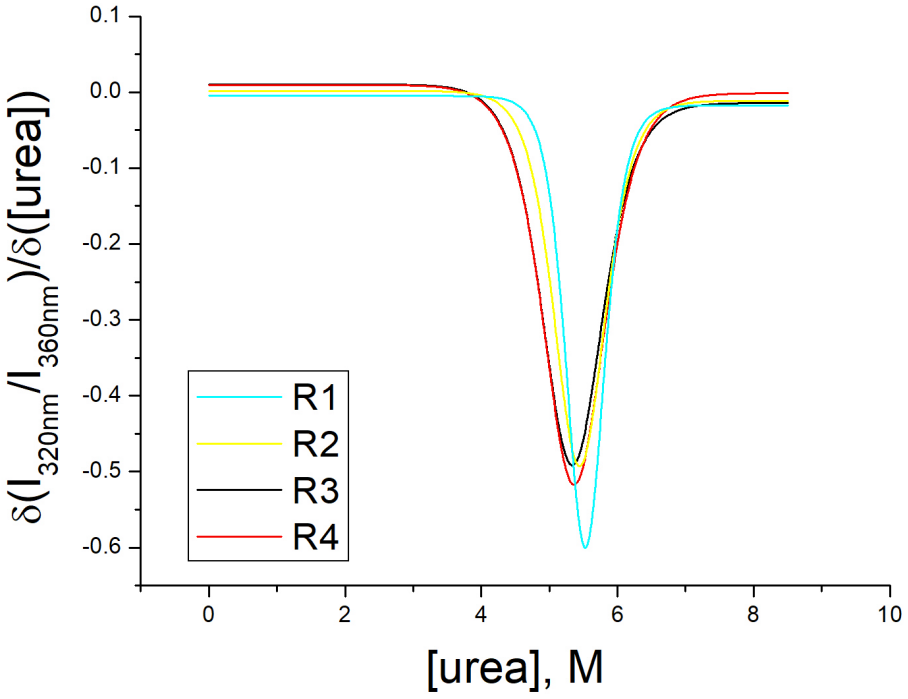

Figure 8. Derivatives of the simulation curves for each replica in the presence of NIH-11

Table 6. *$C_{1/2}$ values obtained for each replica in the presence of NIH-11*

Replica	**1**	**2**	**3**	**4**
$C_{1/2}$, M	**5.52**	**5.45**	**5.34**	**5.36**
			5.35 ± 0.01 M	

As stated in **Table 6**, clear differences were obtained between each ligand concentration, since the bigger ligand concentration induces a bigger stabilization of the domain´s native state and, this is shown in the increase of the urea concentration at the transition point. Nonetheless, because of the lack of time to repeat the experiments, we decided to work with this data and try to obtain the maximum number of valid conclusions from them.

This decision was supported by the fact that, even if this method allows the determination of the dissociation constant from a sole ligand concentration, (Schön et al., 2013) recommend to test several concentrations (normally higher) to assess the stabilization effect. In this case, the concentration of replicas 3 and 4 were lower than the initial proportion of 40x, despite that, the results gave enough information to make an initial estimation of the binding affinity.

- **Binding validation and K_d estimation according to the (Schön et al., 2013) model**

Looking at the results, the binding of NIH-11 to the native state of Tsg101-UEV domain is evident, since there is a clear, if small, increase in the value of $C_{1/2}$ in the presence of NIH-11 (**Figures 9** and **10**).

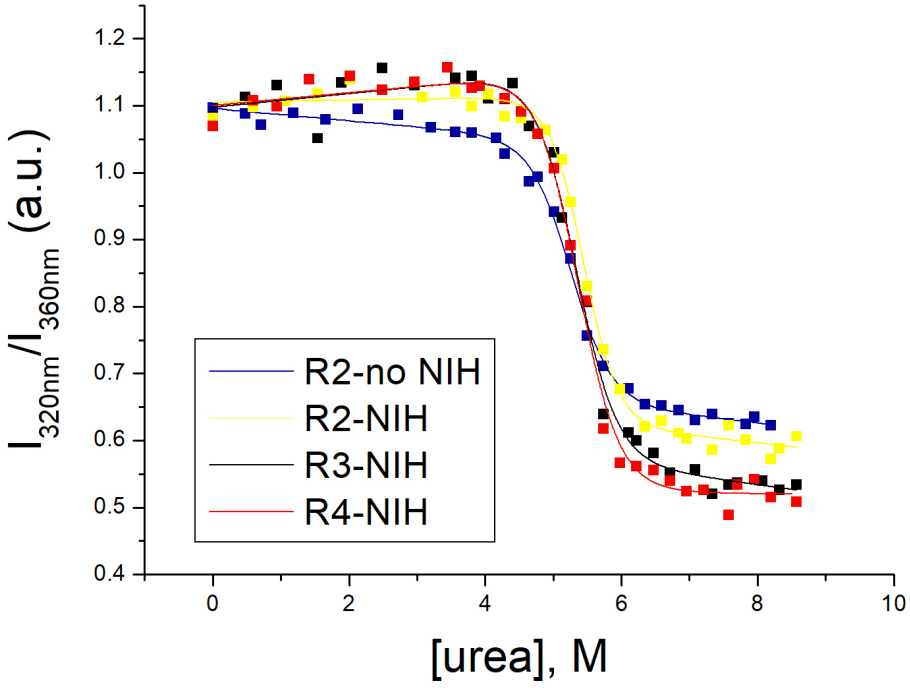

Figure 9. *Comparative of the fitting curves in the absence and presence of NIH-11*

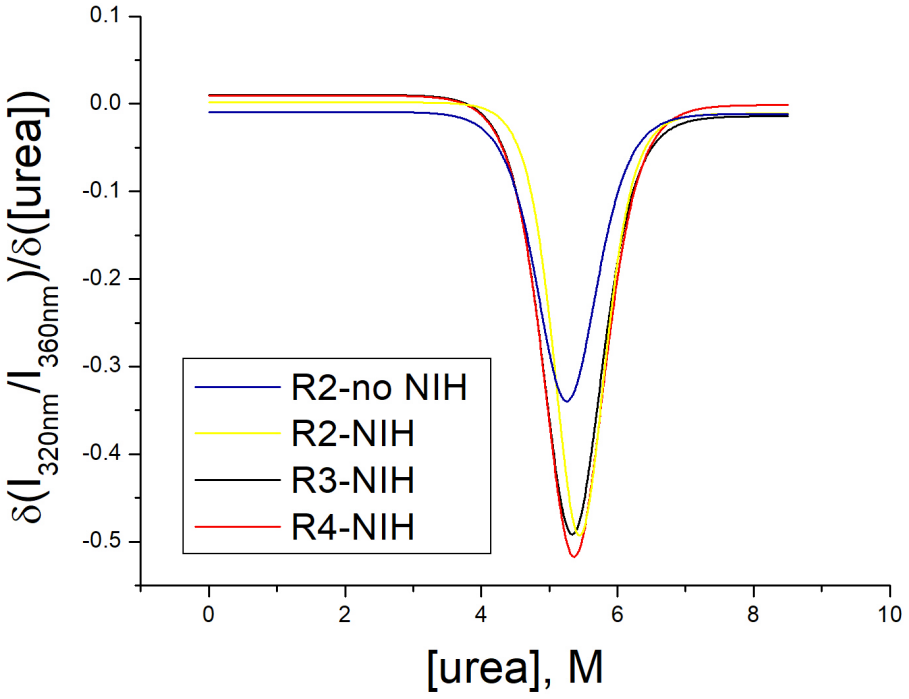

Figure 10. *Comparative of the derivatives in the absence and presence of NIH-11*

The calculation of K_d for the NIH-11 concentrations of 60 and 100 µM (**Table 7**) was obtained using the fitting parameters.

Table 7. *Values of the dissociation constants at 60 and 100 µM of NIH-11*

Replicas	**L_T,** µM	**P_T,** µM	**T**, K	**R**, J/(K·mol)	**m_L,** (J/mol) · M^{-1}	**$\Delta C_{1/2}$,** M	**F**	**K_d,** µM	**K_a,** μM^{-1}
R3, R4	60	2.5	298.15	8.314	8300	0.10	0.4	150	0.007
R2	100	2.5	298.15	8.314	9900	0.20	1.2	81	0.012

The two values obtained for the K_d were in the order of 100 µM, which agrees with the previous values for other polyproline binding domains, which are in the range of 10-300 µM, and they also agree with the values of the natural ligands of Tsg101-UEV (**Table 8**).

Table 8. *Values of binding affinity for the natural ligands of Tsg101-UEV*

Ligand	Sequence	T	K_d	$\Delta G_{binding}$
		K	µM	KJ·mol^{-1}
HIV-9	^{5}PE**P**$_{-3}$ **TAP**$_0$ PEE^{13}	298	71.4	-5.66
HIV-11	^{5}PE**P**$_{-3}$ **TAP**$_0$ PEESF^{15}	298	50.0	-5.86
Ebola-9	^{5}IL**P**$_{-3}$ **TAP**$_0$ PEY^{13}	298	41.7	-5.98
Ebola-11	^{5}IL**P**$_{-3}$ **TAP**$_0$ PEYME^{15}	298	23.3	-6.31
HTLV	^{118}YVE**P**$_{-3}$ **TAP**$_0$ QVL^{127}	298	188.7	-5.07

Nevertheless, both values show between them a difference of approximately the double, an error which agrees with what could be expected. In addition, if we compare these results with the experiments performed by (Schön et al., 2013) (**Table 9**), we can see that we are studying an interaction which is considerably lower. This implies that the effect of the ligand concentration on $\Delta C_{1/2}$ is very small and, therefore, that the calculation of K_d suffers from a bigger uncertainty.

Despite this, if we compare the variation of our K_d with that of the calculated, for instance, for the protein gp120 and the ligand NBD-556 (**Table 9**), there is not a big difference in the value of this variation, even if there is a difference of around an order of magnitude between both constants.

Table 9. *Comparative of the affinity values obtained by (Schön et al., 2013) and those of the Tsg101-UEV/NIH-11 complex*

Protein	**[Protein], µM**	**Ligand**	**[Ligand], µM**	**Denaturant**	**m/m_L**	**$\Delta C_{1/2}$, M**	**ΔG binding, kcal/mol**	**K_d, nM**
hCA-I	0.5	TFMSA	5	Urea	1	1.36	-9.26	163
hCA-I	0.5	TFMSA	10	Urea	1	1.60	-9.20	184
hCA-I	0.5	ACTAZ	200	Urea	1	1.26	-6.9	9,200
HIV-1 PR	0.58	KNI-10769	10	GdnHCl	1	1.03	-10.5	21
HIV-1 PR	0.58	KNI-10006	25	GdnHCl	1	1.64	-13.9	0.063
gp120	0.5	NBD-556	50	Urea	0.72	0.55	-7.2	6,400
gp120	0.5	NBD-556	100	Urea	0.72	0.62	-6.9	8,500
Tsg101-UEV	2.5	NIH-11	60	Urea	1.04	**0.1**	-2.97	150 E3
Tsg101-UEV	2.5	NIH-11	100	Urea	0.87	**0.2**	-2.60	81 E3

After the discussion of these aspects, it is important to highlight that the main goal of this method was not to obtain an exact value of the dissociation constant of the complex, but validating the binding of NIH-11 to Tsg101-UEV, previously observed in the screening campaigns, and establishing the possible order of magnitude for this dissociation constant.

The results obtained here confirm the binding of NIH-11 to Tsg101-UEV domain, based on the mild shift in the urea concentration at the transition point. On the other hand, the exact binding affinity values derived from this method are not so reliable, since the main equations of the model do not have a robust thermodynamic base and it would be necessary to perform more replicas to obtain statistically significant values.

Despite all these aspects, the magnitude of the dissociation constant will be of great importance in the design and optimization of the protocols of more robust and standardized techniques like ITC or the latest MicroScale Thermophoresis (MST) (Jerabek-Willemsen et al., 2014). Future and more exact values of this binding affinity will allow a better comprehension of the nature of this interaction. They will represent a starting point in the computational and experimental improvement of NIH-11´s properties, turning it, hopefully, into a promising broad-spectrum antiviral.

CONCLUSIONS

1) It has been possible to optimise a robust method aimed at validating and estimating the binding affinity of non-peptidic ligands to the Tsg101-UEV domain.

2) For the first time, it has been feasible to estimate the magnitude of the binding affinity associated to one of the several non-peptidic ligands identified by previous in vitro massive campaigns.

3) The binding affinity estimated here is in the order of magnitude expected for Tsg101-UEV and it is similar to previous binding affinities described for its natural ligands.

BIBLIOGRAPHY

https://www.who.int/news-room/fact-sheets/detail/the-top-10-causes-of-death

Anthony S. Fauci, M.D., and David M. Morens, M. D., & A. (2012). The perpetual challenge of infectious diseases. *New England Journal of Medicine*, *366*(5), 454–461. https://doi.org/10.1056/NEJMc1202013

Bagcchi, S. (2020). Lassa fever outbreak continues across Nigeria. *The Lancet Infectious Diseases*, *20*(5), 543. https://doi.org/10.1016/S1473-3099(20)30299-1

Bai, N., Roder, H., Dickson, A., & Karanicolas, J. (2019). Isothermal Analysis of ThermoFluor Data can readily provide Quantitative Binding Affinities. *Scientific Reports*, *9*(1), 1–15. https://doi.org/10.1038/s41598-018-37072-x

Balakin, K. V., Ivanenkov, Y. A., Skorenko, A. V., Nikolsky, Y. V., Savchuk, N. P., & Ivashchenko, A. A. (2004). In silico estimation of DMSO solubility of organic compounds for bioscreening. *Journal of Biomolecular Screening*, *9*(1), 22–31. https://doi.org/10.1177/1087057103260006

Basler, C. F. (2017). Molecular pathogenesis of viral hemorrhagic fever. In *Seminars in Immunopathology*, 39(5), 551–561. Springer Verlag. https://doi.org/10.1007/s00281-017-0637-x

Bouchemal, K. (2008). New challenges for pharmaceutical formulations and drug delivery

systems characterization using isothermal titration calorimetry. In *Drug Discovery Today*, 13(21–22), 960–972. Elsevier Ltd. https://doi.org/10.1016/j.drudis.2008.06.004
Brandts, J. F., & Lin, L. N. (1990). Study of Strong to Ultratight Protein Interactions Using Differential Scanning Calorimetry. *Biochemistry*, *29*(29), 6927–6940. https://doi.org/10.1021/bi00481a024
Bruylants, G., Wouters, J., & Michaux, C. (2005). Differential Scanning Calorimetry in Life Science: Thermodynamics, Stability, Molecular Recognition and Application in Drug Design. *Current Medicinal Chemistry*, *12*, 2011–2020. https://doi.org/10.1111/j.1445-5994.2011.02474.x
Douse, C. H., Vrielink, N., Wenlin, Z., Cota, E., & Tate, E. W. (2015). Targeting a dynamic protein-protein interaction: Fragment screening against the malaria myosin a motor complex. *ChemMedChem*, *10*(1), 134–143. https://doi.org/10.1002/cmdc.201402357
Drury, G., Jolliffe, S., & Mukhopadhyay, T. K. (2019). Process mapping of vaccines: Understanding the limitations in current response to emerging epidemic threats. *Vaccine*, *37*(17), 2415–2421. https://doi.org/10.1016/j.vaccine.2019.01.050
Du, X., Li, Y., Xia, Y. L., Ai, S. M., Liang, J., Sang, P., Ji, X. L., & Liu, S. Q. (2016). Insights into protein–ligand interactions: Mechanisms, models, and methods. In *International Journal of Molecular Sciences*, 17(2). MDPI AG. https://doi.org/10.3390/ijms17020144
Dye, C. (2014). After 2015: Infectious diseases in a new era of health and development. In *Philosophical Transactions of the Royal Society B: Biological Sciences,* 369(1645). Royal Society. https://doi.org/10.1098/rstb.2013.0426
Eisinger, R. W., & Fauci, A. S. (2018). Ending the HIV/AIDS pandemic. *Emerging Infectious Diseases*, *24*(3), 413–416. https://doi.org/10.3201/eid2403.171797
Erlanson, D. A., Fesik, S. W., Hubbard, R. E., Jahnke, W., & Jhoti, H. (2016). Twenty years on: The impact of fragments on drug discovery. *Nature Reviews Drug Discovery*, *15*(9), 605–619. https://doi.org/10.1038/nrd.2016.109
Freire, E. (2015). The Binding Thermodynamics of Drug Candidates. *Thermodynamics and Kinetics of Drug Binding*, 1–13. https://doi.org/10.1002/9783527673025.ch1
Gao, K., Oerlemans, R., & Groves, M. R. (2020). Theory and applications of differential scanning fluorimetry in early-stage drug discovery. In *Biophysical Reviews*, 12(1), 85–104. Springer. https://doi.org/10.1007/s12551-020-00619-2
Greenfield, N. J. (2004). *Circular Dichroism Analysis for Protein–Protein Interactions*. *261*.
Han, Z., Lu, J., Liu, Y., Davis, B., Lee, M. S., Olson, M. A., Ruthel, G., Freedman, B. D., Schnell, M. J., Wrobel, J. E., Reitz, A. B., & Harty, R. N. (2014). Small-Molecule Probes Targeting the Viral PPxY-Host Nedd4 Interface Block Egress of a Broad Range of RNA Viruses. *Journal of Virology*, *88*(13), 7294–7306. https://doi.org/10.1128/jvi.00591-14
Ilunga Kalenga, O., Moeti, M., Sparrow, A., Nguyen, V.-K., Lucey, D., & Ghebreyesus, T. A. (2019). The Ongoing Ebola Epidemic in the Democratic Republic of Congo, 2018–2019. *New England Journal of Medicine*, *381*(4), 373–383. https://doi.org/10.1056/NEJMsr1904253
Im, Y. J., Kuo, L., Ren, X., Burgos, P. V., Zhao, X. Z., Liu, F., Burke, T. R., Bonifacino, J. S., Freed, E. O., & Hurley, J. H. (2010). Crystallographic and Functional Analysis of the ESCRT-I /HIV-1 Gag PTAP Interaction. *Structure*, *18*(11), 1536–1547. https://doi.org/10.1016/j.str.2010.08.010
Jerabek-Willemsen, M., André, T., Wanner, R., Roth, H. M., Duhr, S., Baaske, P., &

Breitsprecher, D. (2014). MicroScale Thermophoresis: Interaction analysis and beyond. *Journal of Molecular Structure*, *1077*, 101–113. https://doi.org/10.1016/j.molstruc.2014.03.009
Kranz, J. K., & Schalk-Hihi, C. (2011). Protein Thermal Shifts to Identify Low Molecular Weight Fragments. In *Methods in Enzymology*, 493, 277–298. Academic Press Inc. https://doi.org/10.1016/B978-0-12-381274-2.00011-X
Lederberg, J., Shope, R. E., & Stanley C. Oaks, J. (1992). *Emerging Infections*. National Academies Press. https://doi.org/10.17226/2008
Mäntele, W., & Deniz, E. (2017). UV–VIS absorption spectroscopy: Lambert-Beer reloaded. *Spectrochimica Acta - Part A: Molecular and Biomolecular Spectroscopy*, *173*, 965–968. https://doi.org/10.1016/j.saa.2016.09.037
Martin-Serrano, J., & Neil, S. J. D. (2011). Host factors involved in retroviral budding and release. *Nature Reviews Microbiology*, *9*(7), 519–531. https://doi.org/10.1038/nrmicro2596
Martinez, J. P., Sasse, F., Brönstrup, M., Diez, J., & Meyerhans, A. (2015). Antiviral drug discovery: Broad-spectrum drugs from nature. In *Natural Product Reports*, 32(1), 29–48. Royal Society of Chemistry. https://doi.org/10.1039/c4np00085d
Mocz, G., & Ross, J. A. (2013). Fluorescence techniques in analysis of protein-ligand interactions. *Methods in Molecular Biology*, *1008*, 169–210. https://doi.org/10.1007/978-1-62703-398-5_7
Monera, O. D., Kay, C. M., & Hodges, R. S. (1994). Protein denaturation with guanidine hydrochloride or urea provides. *Protein Science*, *3*(11), 1984–1991.
Morens, D. M., Folkers, G. K., & Fauci, A. S. (2008). Emerging infections: a perpetual challenge. In *The Lancet Infectious Diseases*, 8(11), 710–719. Elsevier. https://doi.org/10.1016/S1473-3099(08)70256-1
Myers, J. K., Nick Pace, C., & Martin Scholtz, J. (1995). Denaturant m values and heat capacity changes: Relation to changes in accessible surface areas of protein unfolding. *Protein Science*, *4*(10), 2138–2148. https://doi.org/10.1002/pro.5560041020
Nii-Trebi, N. I. (2017). Emerging and Neglected Infectious Diseases: Insights, Advances, and Challenges. *BioMed Research International*, *2017*. https://doi.org/10.1155/2017/5245021
Oyston, P., & Robinson, K. (2012). The current challenges for vaccine development. In *Journal of Medical Microbiology*, 61(PART7), 889–894. Microbiology Society. https://doi.org/10.1099/jmm.0.039180-0
Pace, C. N. (1990). Conformational stability of globular proteins. In *Trends in Biochemical Sciences*, 15(1), 14–17. Elsevier Current Trends. https://doi.org/10.1016/0968-0004(90)90124-T
Pace, C. N., Vajdos, F., Fee, L., Grimsley, G., & Gray, T. (1995). How to measure and predict the molar absorption coefficient of a protein. *Protein Science*, *4*(11), 2411–2423. https://doi.org/10.1002/pro.5560041120
Palencia, A., Martinez, J. C., Mateo, P. L., Luque, I., & Camara-Artigas, A. (2006). Structure of human TSG101 UEV domain. *Acta Crystallographica Section D: Biological Crystallography*, *62*(4), 458–464. https://doi.org/10.1107/S0907444906005221
Pavia, A. T. (2007). Germs on a Plane: Aircraft, International Travel, and the Global Spread of Disease. *The Journal of Infectious Diseases*, *195*(5), 621–622. https://doi.org/10.1086/511439
Pornillos, O., Garrus, J. E., & Sundquist, W. I. (2002). Mechanisms of enveloped RNA virus

budding. *Trends in Cell Biology*, *12*(12), 569–579. https://doi.org/10.1016/S0962-8924(02)02402-9
Privalov, P. L. (1979). Stability of proteins: Small Globular Proteins. *Advances in Protein Chemistry*, *33*(C), 167–241. https://doi.org/10.1016/S0065-3233(08)60460-X
Reina, J. (2020). El SARS-CoV-2, una nueva zoonosis pandémica que amenaza al mundo. *Vacunas*, *x x*, 1–6. https://doi.org/10.1016/j.vacun.2020.03.001
Schmid, F., & Beer, L. (2001). Biological Macromolecules : Spectrophotometry Concentrations. *Methods*, 1–4.
Schmidt, O., & Teis, D. (2012). The ESCRT machinery. *Current Biology*, *22*(4), R116–R120. https://doi.org/10.1016/j.cub.2012.01.028
Schön, A., Brown, R. K., Hutchins, B. M., & Freire, E. (2013). Ligand binding analysis and screening by chemical denaturation shift. *Analytical Biochemistry*, *443*(1), 52–57. https://doi.org/10.1016/j.ab.2013.08.015
Tavassoli, A., Lu, Q., Gam, J., Pan, H., Benkovic, S. J., & Cohen, S. N. (2008). Inhibition of HIV budding by a genetically selected cyclic peptide targeting the Gag-TSG101 interaction. *ACS Chemical Biology*, *3*(12), 757–764. https://doi.org/10.1021/cb800193n
Tjernberg, A., Markova, N., Griffiths, W. J., & Hallén, D. (2006). DMSO-Related Effects in Protein Characterization. *Journal of Biomolecular Screening*, *11*(2), 131–137. https://doi.org/10.1177/1087057105284218
Vuignier, K., Schappler, J., Veuthey, J. L., Carrupt, P. A., & Martel, S. (2010). Drug-protein binding: A critical review of analytical tools. In *Analytical and Bioanalytical Chemistry*, 398(1), 53–66. Springer. https://doi.org/10.1007/s00216-010-3737-1
Waldron, T. T., & Murphy, K. P. (2003). Stabilization of proteins by ligand binding: Application to drug screening and determination of unfolding energetics. *Biochemistry*, *42*(17), 5058–5064. https://doi.org/10.1021/bi034212v
Warren, J. R., & Gordon, J. A. (1966). On the refractive indices of aqueous solutions of urea. *Journal of Physical Chemistry*, *70*(1), 297–300. https://doi.org/10.1021/j100873a507
Williamson, M. P. (2013). Using chemical shift perturbation to characterise ligand binding. In *Progress in Nuclear Magnetic Resonance Spectroscopy*, 73, 1–16. Elsevier B.V. https://doi.org/10.1016/j.pnmrs.2013.02.001
Yun, J., Yu, O., & Xiaodong, C. (2013). Role of TSG101 in cancer Yun. *Frontiers in Bioscience*, *18*, 279–288. https://doi.org/10.3969/j.issn.1001-1242.2013.07.020